scientific reports

Check for updates

OPEN

Hypoxia-mediated rescue of retinal ganglion cells deficient in mitochondrial complex I is independent of the hypoxia-inducible factor pathway

Alexander M. Warwick[1], Howard M. Bomze[1], Luyu Wang[1], Ying Hao[1], Sandra S. Stinnett[1] & Sidney M. Gospe III[1,2]✉

Continuous exposure to environmental hypoxia (11% O_2) has been shown to markedly slow the progressive degeneration of retinal ganglion cells (RGCs) in a mouse model of mitochondrial optic neuropathy with RGC-specific deletion of the key mitochondrial complex I accessory subunit *ndufs4*. As a first step toward identifying the therapeutic mechanism of hypoxia in this model, we conducted a series of experiments to investigate the role of the hypoxia-inducible factor (HIF) regulatory pathway in RGC neuroprotection. *Vglut2-Cre; ndufs4*$^{loxP/loxP}$ mice were crossed with strains bearing *floxed* alleles of the negative HIF regulatory *vhl* or of the two major HIF α-subunit isoforms, *Hif1α* and *Hif2α*. Deletion of *vhl* within *ndufs4*-deficient RGCs failed to prevent RGC degeneration under normoxia, indicating that HIF activation is not sufficient to achieve RGC rescue. Furthermore, the rescue of *ndufs4*-deficient RGCs by hypoxia remained robust despite genetic inactivation of *Hif1α* and *Hif2α*. Our findings demonstrate that the HIF pathway is entirely dispensable to the rescue of RGCs by hypoxia. Future efforts to uncover key HIF-independent molecular pathways induced by hypoxia in this mouse model may be of therapeutic relevance to mitochondrial optic neuropathies such as Leber hereditary optic neuropathy.

Keywords Hypoxia, Mitochondria, Complex I, Leber hereditary optic neuropathy, Retinal ganglion cell, Hypoxia-inducible factor

Many retinal and optic nerve disorders arise due to mitochondrial dysfunction, either as a primary heritable condition or as an acquired pathology[1–4]. A particularly debilitating mitochondrial optic neuropathy is Leber hereditary optic neuropathy (LHON), which manifests as subacute profound bilateral vision loss, typically striking patients in adolescence or young adulthood and resulting in legal blindness in the majority of cases[5]. Following a mitochondrial inheritance pattern with variable penetrance, most cases of LHON are caused by hypomorphic mutations in mitochondrial DNA (mtDNA) encoding one of the subunits of mitochondrial respiratory complex I[6]. The resulting partial loss of function of complex I leads to the degeneration of retinal ganglion cells (RGCs), the axons of which form the optic nerve and project to the brain. Interestingly, RGCs appear to be unique in their sensitivity to complex I deficiency, as patients with LHON commonly present with vision loss as an isolated symptom[7]. RGC degeneration is believed to occur due to a combination of reduced ATP generating capacity and increased reactive oxygen species formation, both resulting from a dysfunctional electron transport chain[8–10].

Progress in developing therapies for LHON and other mitochondrial diseases has been slow, owing in part to the technical difficulty of manipulating the mitochondrial genome to generate relevant animal models. Previous genetically modified mouse models of LHON demonstrated a significant latency in the development of RGC degeneration, failing to manifest overt optic atrophy until 1–2 years of age[11–13]. This led us to develop an in vivo model of mitochondrial optic neuropathy with more severe loss-of-function of complex I by using Cre recombinase driven by the vesicular glutamate transporter Vglut2 to achieve RGC-specific deletion of a

[1]Department of Ophthalmology, Duke University School of Medicine, Durham, NC 27710, USA. [2]Department of Ophthalmology, Box 3712 Med Center, Duke University, 2351 Erwin Road, Durham, NC 27710, USA. ✉email: smg4@duke.edu

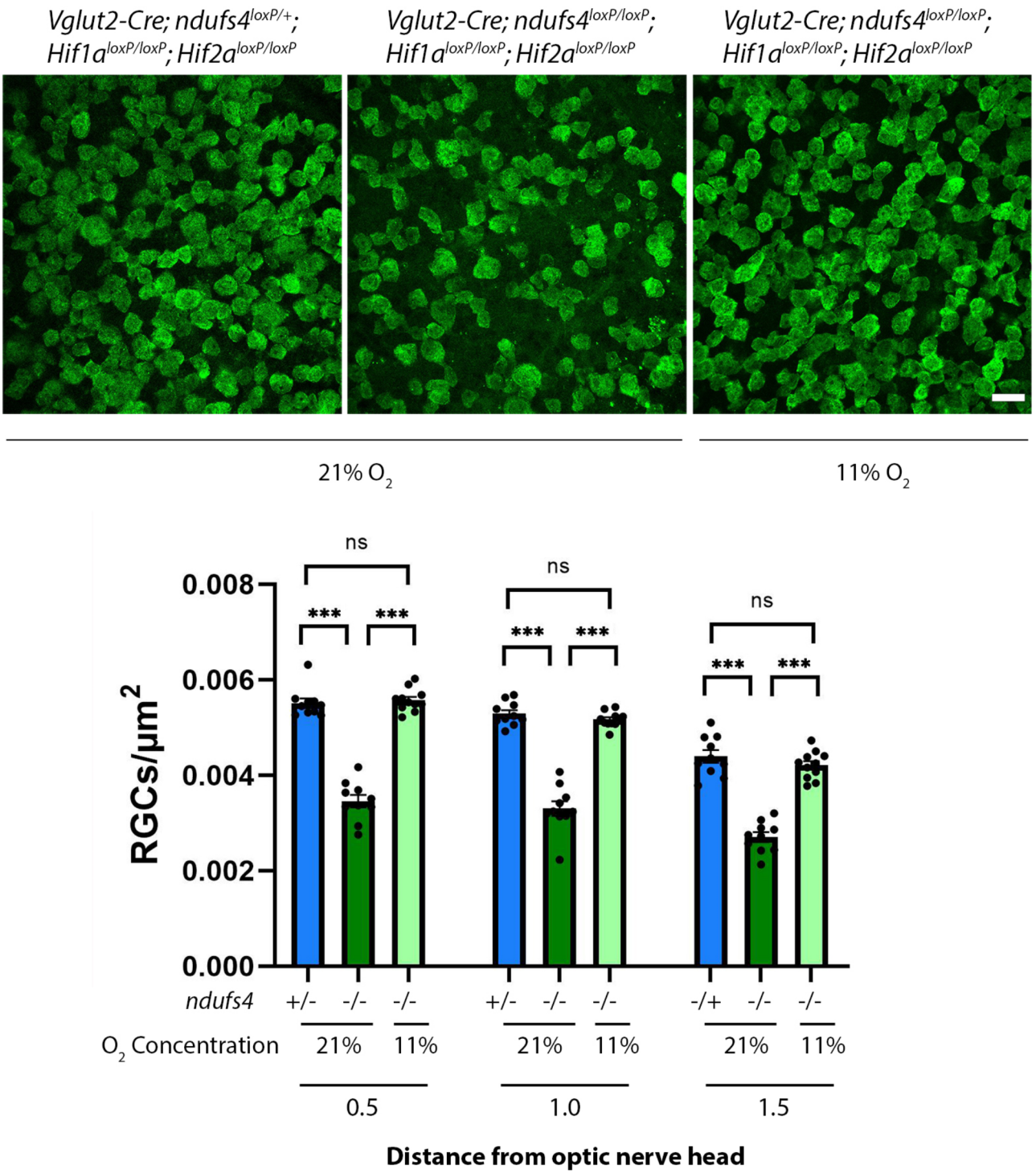

nuclear-encoded accessory subunit of complex I, NADH: ubiquinone oxidoreductase subunit S4 (NDUFS4)[14]. In this *Vglut2-Cre; ndufs4*$^{loxP/loxP}$ mouse line, RGCs lacking the *ndufs4* gene exhibit the onset of degeneration between postnatal days 30 and 45 (P30-45), with RGC loss progressing to approximately two-thirds by P90. The efficiency of RGC degeneration in this mouse model and the fact that it begins around the time of sexual maturity, similar to many human LHON cases, supports its use as a preclinical model for studying potential therapies for mitochondrial optic neuropathy.

Inspired by reports of a substantial rescue of the neurological dysfunction and the shortened lifespan of mice with germline deletion of *ndufs4* when they are raised under continuous hypoxia[15–17], we recently evaluated the potential neuroprotective effect of hypoxia in our RGC-specific *ndufs4* knockout line[18]. Exposure of these mice to 11% O_2 starting at P25, prior to the onset of RGC degeneration, resulted in complete rescue of degeneration at P60, when one-third of RGCs would have otherwise died. By P90, the neuroprotective effect of continuous hypoxia was no longer complete, but nevertheless decreased RGC degeneration by 50%.

◀**Fig. 1**. Deletion of *vhl* does not prevent degeneration of *ndufs4*-deficient retinal ganglion cells. (A) To assess for cell-specific recombination of floxed *vhl*, a flattened retina from a *Vglut2-Cre;vhl*$^{loxP/loxP}$ mouse was serially sectioned in 40-µm increments to collect tissue from the outermost to the innermost retinal layers (samples 1–5). PCR was performed on purified genomic DNA from each section to reveal the presence of *vhl*$^{loxP/loxP}$ that is non-recombined (2 *loxP* sites, 460 bp) and recombined (1 *loxP* site, 260 bp). The presence of the Vglut2-Cre transgene in the genomic DNA was also confirmed by PCR. The schematics to the right depict the beginning of the *vhl* locus pre- and post-recombination, showing the positions of the loxP sites flanking Exon 1 and the expected PCR product sizes resulting from a reaction in which two forward primers (F1 and F2) and one common reverse primer (Rcomm) are used. See Supplementary Fig. S1 online for un-cropped gels. (B, C) Representative images of retinal flat mounts from control mice without the Cre transgene (left panel) and from mice with the indicated heterozygosity or homozygosity status for deletion of *ndufs4* and *vhl* from RGCs at (B) P30 and (C) P45 time points. RGCs are immunolabeled with RNA-Binding Protein 1 (RBPMS1, green). Bar, 20 µm. In each graph below, the density of RGC somas for each genotype is quantified at distances of 0.5, 1.0, and 1.5 mm from the optic nerve head. Individual data points are overlaid on each bar. Statistical comparisons between groups are indicated above the bars, with the following significance designations: ns, not significant; *, $p < 0.05$; **, $p < 0.01$; ***, $p < 0.001$.

Although the beneficial effect of hypoxia on mice with global and RGC-specific mitochondrial dysfunction was considerable, the requirement for continuous administration likely precludes its usefulness as a viable therapy for human disease[15]. Uncovering the mechanism(s) of hypoxia-mediated RGC rescue is therefore a crucial next step, potentially allowing for the identification of key molecular pathways that could by modulated pharmacologically to achieve similar neuroprotective effects under normoxia. A logical starting point is the evaluation of the hypoxia-inducible factor (HIF) family of transcription factors, which collectively serve as the major mediator of many cellular and physiological adaptations to hypoxia[19]. In the present investigation, we reasoned that therapeutic strategies that enhance HIF activity or that stimulate specific HIF-dependent pathways could reproduce the neuroprotective effect of hypoxia. However, we report that HIF pathway activation is neither sufficient nor necessary for rescue of RGCs with intrinsic complex I dysfunction. Our observations indicate that the salutary effect of hypoxia occurs either through a HIF-independent mechanism or is mediated by non-RGC cells that are not subjected to mitochondrial dysfunction or HIF modulation in our model.

Results

Loss of the HIF negative regulator pVHL fails to rescue ndufs4-deficient RGCs under normoxia

We first set out to test whether the neuroprotective effect of hypoxia on *ndufs4*-deficient RGCs is explained entirely by activation of the HIF regulatory pathway within RGCs. The diverse transcriptional program controlled by the HIF family of transcription factors facilitates a number of cellular adaptations to hypoxia, including metabolic reprogramming to favor glycolysis over oxidative metabolism, up-regulation of antioxidants, and the production of paracrine and endocrine signals such as vascular endothelial growth factor and erythropoetin[20,21]. Manipulating RGCs to broadly activate this transcriptional program could theoretically achieve a similar level of neuroprotection as hypoxia itself.

While pharmacological activators of the HIF pathway exist, we reasoned that a genetic approach to activate HIF constitutively would provide the most unambiguous results, by obviating any concerns about blood/brain barrier penetration of pharmacological agents. Constitutive HIF activation can be accomplished by ablating a negative regulator of the HIF proteins. HIF transcription factors are heterodimers consisting of an α- and β-subunit. Under normoxia, the HIF α-subunit is constitutively hydroxylated by prolyl hydroxylase enzymes in an O_2-dependent reaction and then targeted for proteolysis by the von-Hippel lindau protein (pVHL), an E3 ubiquitin ligase[22]. Under hypoxia, the HIF α-subunit cannot be hydroxylated and degraded and may therefore translocate to the nucleus, bind the β-subunit, and up-regulate HIF target genes. Deletion of the *vhl* gene encoding pVHL is a common approach to promote HIF stabilization and transcriptional activity under normoxia, but because *vhl* deletion results in embryonic lethality[23], in vivo studies require a conditional knockout approach.

To achieve a cell-specific knockout of *vhl* within metabolically impaired RGCs lacking NDUFS4, we crossed *Vglut2-Cre; ndufs4*$^{loxP/loxP}$ mice with a transgenic line bearing *floxed* alleles of *vhl* (*vhl*$^{loxP/loxP}$).[24] Because RGCs comprise only ~ 1% of all retinal cells[25], confirming loss of pVHL protein by Western blot was not feasible, and we could not find a suitable antibody to assess pVHL expression by immunofluorescence. Therefore, we adapted the method of Grimm and colleagues to assess for recombination of *floxed vhl* as an indicator of successful Cre-mediated deletion of the gene[26]. Because *Vglut2*-driven expression of Cre in the retina occurs almost exclusively within RGCs (it may also occur in < 10% of cones and horizontal cells)[14], we would expect to find evidence of *vhl*$^{loxP/loxP}$ recombination primarily in the ganglion cell layer of the retina. In order to assess for this, we collected tissue from different retinal layers by adapting a well-established serial sectioning technique on retinal flat mounts;[27] however, in our case, rather than collecting fine 5–10 µm sections through photoreceptor subcompartments, we obtained thicker 40 µm sections to more broadly divide up the full thickness of the retina. We then performed PCR to profile *vhl*$^{loxP/loxP}$ recombination in nuclear DNA obtained from different retinal layers from *Vglut2-Cre; vhl*$^{loxP/loxP}$ mice. As expected, the DNA of the Cre transgene was detectable in the nuclear DNA of cells throughout the retina; however, the cell-specific *Vglut2*-driven expression of Cre recombinase resulted in the vast majority of Cre-mediated recombination of *floxed vhl* occuring within the the inner fifth of the retina, where RGCs reside (Fig. 1A). Even in the ganglion cell layer, RGCs constitute no more than 50% of all cells present[28], so it was not surprising that non-recombined *floxed vhl* remained detectable in the inner-

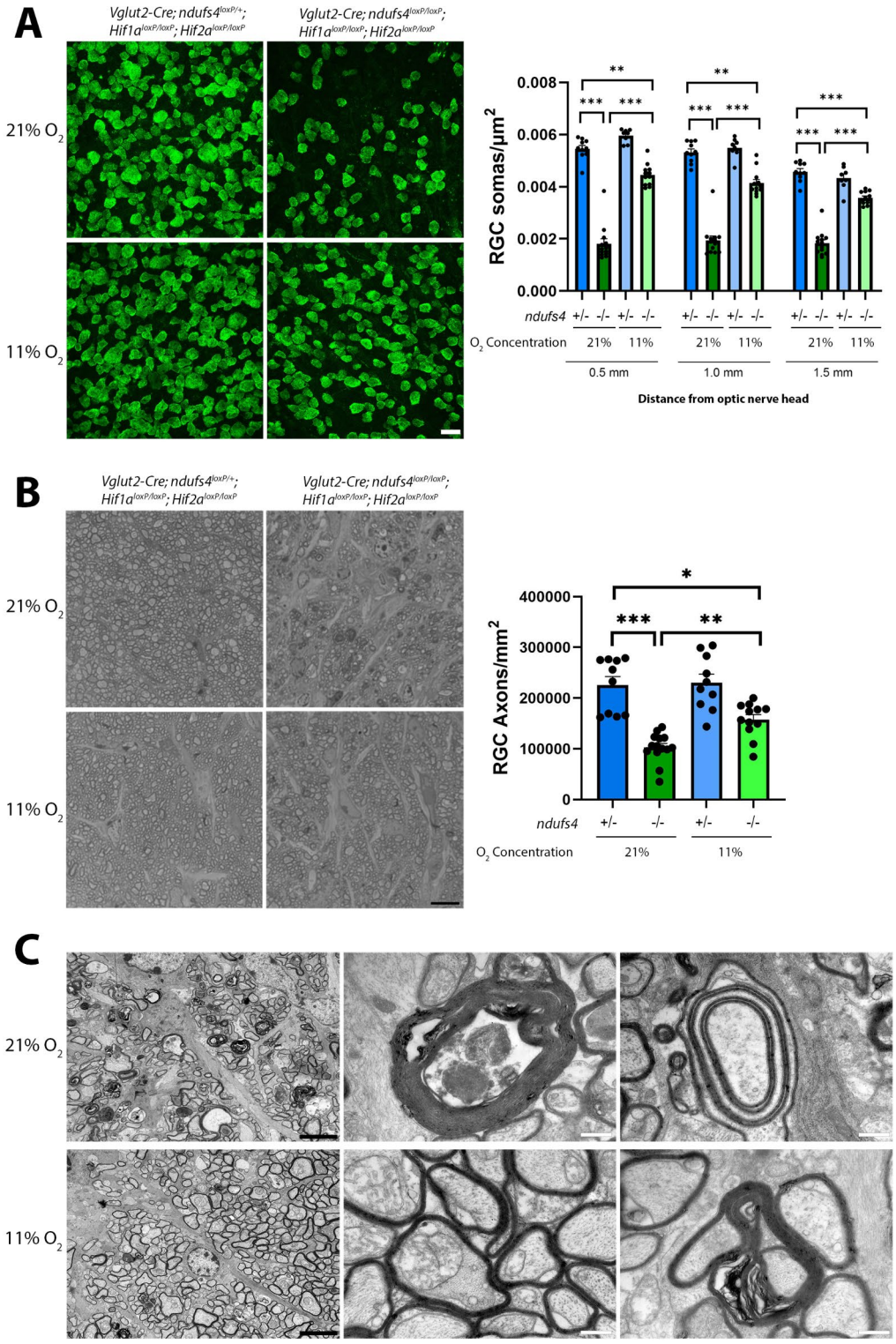

most section. Note that the PCR analysis relied on separate forward primers to detect the recombined and non-recombined *floxed vhl* alleles (Fig. 1A; schematic), meaning that band intensities for each cannot be directly compared quantitatively.

We next proceeded to assess RGC soma degeneration in retinal flat mounts from *Vglut2-Cre; ndufs4*$^{loxP/loxP}$;*vhl*$^{loxP/loxP}$ mice. In our previous characterizations of *Vglut2-Cre; ndufs4*$^{loxP/loxP}$ mice, we have typically performed histological analyses at P60 and P90, because analysis at even later time points is precluded by a progressive and ultimately fatal neurological dysfunction that develops in these mice due to Cre expression in a subset of glutmatergic neurons of the central nervous system[14,29]. Somewhat surprisingly, we found that the combination of *Vglut2-Cre*-mediated deletion of both *ndufs4* and *vhl* genes greatly hastened the progression of neurological morbidity in *Vglut2-Cre; ndufs4*$^{loxP/loxP}$;*vhl*$^{loxP/loxP}$ mice, preventing their survival even to P60. Therefore, we conducted our analysis at the earlier time points of P30 and P45, at which we have previously

◀**Fig. 2**. Retinal ganglion cell-specific deletion of *Hif1α and Hif2α*. (A) To confirm cell-specific recombination of *floxed Hif1α* and *Hif2α*, a flattened retina from a *Vglut2-Cre; Hif1α*$^{loxP/loxP}$;*Hif2α*$^{loxP/loxP}$ mouse was serially sectioned in 40-µm increments to collect tissue from the outermost to the innermost retinal layers (samples 1–5). PCR was performed on purified genomic DNA from each section to demonstrate the presence of *Hif1α*$^{loxP/loxP}$ and *Hif2α*$^{loxP/loxP}$ alleles that are non-recombined (2 *loxP* sites) and recombined (1 *loxP* site). The presence of the *Vglut2-Cre* transgene in the genomic DNA was also confirmed by PCR. The schematics to the right depict the beginning of the *floxed Hif1α* and *Hif2α loci* pre- and post-recombination, showing the positions of the loxP sites flanking Exon 2 of each gene. The positions of each of the two forward primers (F1 and F2) and one common reverse primer (Rcomm) used for each gene are also depicted, as well as the expected PCR product sizes for each reaction when all three primers are combined. Note that for *Hif1α*, the locations of the forward primers relative to each loxP site result in the post-recombination amplification product being slightly larger than for the non-recombined product. See Supplementary Fig. S2 online for un-cropped gels. (B) Retinal flat mount from a P60 *Vglut2-Cre; Hif1α*$^{loxP/loxP}$;*Hif2α*$^{loxP/loxP}$ mouse stained for RBPMS1 demonstrates healthy RGC soma morphology and density. Bar, 20 µm. (C) Electron micrograph of an optic nerve cross section from a P60 *Vglut2-Cre; Hif1α*$^{loxP/loxP}$;*Hif2α*$^{loxP/loxP}$ mouse demonstrates abundant RGC axons with normal myelination. Bar, 5 µm.

reported that *Vglut2-Cre; ndufs4*$^{loxP/loxP}$ mice with intact *vhl* show no RGC degeneration (P30) and very mild degeneration (P45).

As a normal control, we used *ndufs4*$^{loxP/loxP}$;*vhl*$^{loxP/loxP}$ mice with *floxed* alleles of *ndufs4* and *vhl*, but no Cre recombinase. We also included a cohort of *Vglut2-Cre; ndufs4*$^{loxP/+}$;*vhl*$^{loxP/+}$ mice, which are heterozygous for *floxed* alleles of both *ndufs4* and *vhl* and were expected to be aphenotypic because they retain one intact copy of each gene. In addition to *Vglut2-Cre; ndufs4*$^{loxP/loxP}$;*vhl*$^{loxP/loxP}$ mice lacking both copies of *ndufs4* and *vhl*, we also included *Vglut2-Cre; ndufs4*$^{loxP/loxP}$;*vhl*$^{loxP/+}$ and *Vglut2-Cre; ndufs4*$^{loxP/+}$;*vhl*$^{loxP/loxP}$ mice, so that the effects of homozygous deletion of *ndufs4* or *vhl*, respectively, could be assessed separately. At P30 we found that homozygous deletion of either *ndufs4* or *vhl* had no effect on RGC soma survival, as expected (Fig. 1B). Interestingly, and contrary to the notion that constitutive HIF activation would be beneficial in the setting of *ndufs4* deficiency, there was a small decrease in RGC survival in P30 *Vglut2-Cre; ndufs4*$^{loxP/loxP}$;*vhl*$^{loxP/loxP}$ double knockout mice that reached statistical significance at locations of 0.5 mm and 1.0 mm, but not 1.5 mm, from the optic nerve head. At the later time point of P45, the *Vglut2-Cre; ndufs4*$^{loxP/loxP}$;*vhl*$^{loxP/+}$ mice with both copies of *ndufs4* deleted from RGCs exhibited the expected small reduction of survival of RGC somas by ~ 20% at all three retinal locations (Fig. 1C). When both copies of *vhl* were deleted alongside *ndufs4* in RGCs, the degeneration of RGC somas at P45 was unmitigated. Thus, it appears that deletion of the HIF negative regulator *vhl* does not produce a neuroprotective effect on RGCs equivalent to hypoxia. Indeed, the rapid deterioration of the systemic health of the mice with both *ndufs4* and *vhl* deleted from glutamatergic neurons suggests that artificial HIF activation may be deleterious in this context. This observation is consistent with a recent report that combining the global knockout of *ndufs4* with null alleles of various prolyl hydroxylase enzymes or a hypomorphic *vhl* mutation failed to extend and in some instances reduced the lifespan of the mice[30].

Rescue of ndufs4-deficient RGCs by hypoxia is independent of HIF pathway activation

Our analysis of mice with conditional deletion of *vhl* suggested that activation of the HIF regulatory pathway is not sufficient for rescue of RGCs with complex I impairment, but it did not necessarily indicate that the HIF pathway is unnecessary for RGC rescue by hypoxia. Because systemic ablation of the HIF pathway is embryonically lethal[31,32], formal testing of the dependence of hypoxia-mediated rescue of *ndufs4* global knockout mice on HIF activation has not been conducted by other laboratories. However, our mouse model of tissue-specific genetic ablation provided an ideal opportunity to pursue this question. We therefore proceeded to use the *Vglut2-Cre* line to inactivate the HIF pathway in the same RGCs that have lost *ndufs4* and to determine whether chronic hypoxia remained neuroprotective.

The key players in the HIF-mediated physiological response to hypoxia are HIF-1 and HIF-2 (with the final member, HIF-3, inhibiting their actions)[20,21,33]. Each has a unique α-subunit, while sharing a common β-subunit. Because of their partial redundancy[34], it was important to abrogate the function of both HIF-1α and HIF-2α in order to comprehensively test the necessity of HIF activation in the salutary effect of hypoxia on RGCs. Therefore, we employed genetically modified mouse lines with *floxed Hif1α*[35] and *Hif2α*[36] alleles, allowing for deletion of both genes within RGCs when bred with the *Vglut2-Cre* line. As with deletion of *vhl*, demonstration of RGC-specific depletion of the HIF proteins is challenging, particularly given that the rapid degradation of HIF-1α and HIF-2α means that they are not abundantly expressed in wild type retina. Instead, to confirm successful Cre-mediated recombination of the *floxed Hif1α* and *Hif2α* alleles within RGCs, we again obtained serial tangential sections of retinal flat mounts and observed the expected Cre-mediated recombination of *floxed Hif1α* and *Hif2α* almost exclusively in the inner-most retinal layer of *Vglut2-Cre; Hif1α*$^{loxP/loxP}$;*Hif2α*$^{loxP/loxP}$ mice (Fig. 2A). We examined RGC soma and axon histology on retinal flat mounts and optic nerve cross sections of these mice at P60 and confirmed that RGC morphology and abundance appeared normal, indicating that the embryonic ablation of the HIF pathway in RGCs was not detrimental to their development (Fig. 2B, C).

We next generated *Vglut2-Cre; ndufs4*$^{loxP/loxP}$;*Hif1α*$^{loxP/loxP}$;*Hif2α*$^{loxP/loxP}$ mice with triple-knockout of *ndufs4*, *Hif1α* and *Hif2α* in RGCs and raised these mice under either normoxia (21% O_2) or hypoxia (11% O_2) beginning at P25. Having already confirmed that deletion of *Hif1α* and *Hif2α* did not lead to overt RGC degeneration, we used as control littermates *Vglut2-Cre; ndufs4*$^{loxP/+}$;*Hif1α*$^{loxP/loxP}$;*Hif2α*$^{loxP/loxP}$ mice in which RGCs lacked both

copies of *Hif1α* and *Hif2α* but maintained one intact copy of *ndufs4*. When ocular tissues were harvested at P60 from mice raised under normoxia, we observed the expected reduction of RGC soma density in the retinas of *Vglut2-Cre; ndufs4*$^{loxP/loxP}$;*Hif1α*$^{loxP/loxP}$;*Hif2α*$^{loxP/loxP}$ mice lacking both copies of *ndufs4* within RGCs compared to the heterozygous controls (Fig. 3). However, in those mice raised under continuous hypoxia, there was no difference in RGC soma density between *Vglut2-Cre; ndufs4*$^{loxP/loxP}$;*Hif1α*$^{loxP/loxP}$;*Hif2α*$^{loxP/loxP}$ mice and *Vglut2-Cre; ndufs4*$^{loxP/+}$;*Hif1α*$^{loxP/loxP}$;*Hif2α*$^{loxP/loxP}$ controls, indicating that despite ablation of the HIF pathway within RGCs, therapeutic hypoxia remained 100% neuroprotective at this time point.

We performed a similar analysis at the later time point of P90, at which we had previously observed a durable but incomplete neuroprotective effect of hypoxia in *Vglut2-Cre; ndufs4*$^{loxP/loxP}$ mice with an intact HIF pathway[18]. This partial rescue of RGC somas was preserved in *Vglut2-Cre; ndufs4*$^{loxP/loxP}$;*Hif1α*$^{loxP/loxP}$;*Hif2α*$^{loxP/loxP}$ mice raised in hypoxia from P25 to P90 (Fig. 4A). While there was a reduction in RGC soma survival in these hypoxia-raised triple-knockout mice compared to control littermates with one intact copy of *ndufs4*, the degeneration of RGCs was reduced by well over 50% at all three distances from the optic nerve head compared to *Vglut2-Cre; ndufs4*$^{loxP/loxP}$;*Hif1α*$^{loxP/loxP}$;*Hif2α*$^{loxP/loxP}$ mice raised entirely under normoxia. To confirm that the therapeutic effect of hypoxia on complex I-deficient RGCs extended to survival of their axons, we harvested optic nerves from these same mice and quantified axon density in optic nerve cross sections. Similar to our analysis of RGC somas, we observed a significant but incomplete reduction of axon degeneration at P90 in *Vglut2-Cre; ndufs4*$^{loxP/loxP}$;*Hif1α*$^{loxP/loxP}$;*Hif2α*$^{loxP/loxP}$ mice exposed to continuous hypoxia (Fig. 4B). Ultrastructural analysis with transmission electron microscopy showed that in addition to a reduced abundance of axons, the optic nerves from *Vglut2-Cre; ndufs4*$^{loxP/loxP}$;*Hif1α*$^{loxP/loxP}$;*Hif2α*$^{loxP/loxP}$ mice raised under normoxia exhibited highly abnormal myelination patterns, with myelin sheaths that were thickened, duplicated, or shared between multiple axons (Fig. 4C). Consistent with our previous observations in *Vglut2-Cre; ndufs4*$^{loxP/loxP}$ mice, these abnormal morphological findings were substantially less common when the *Vglut2-Cre; ndufs4*$^{loxP/loxP}$ mice were raised under hypoxia. Altogether, the salutary effect of continuous hypoxia appeared to be entirely unaffected by ablation of the HIF pathway within RGCs.

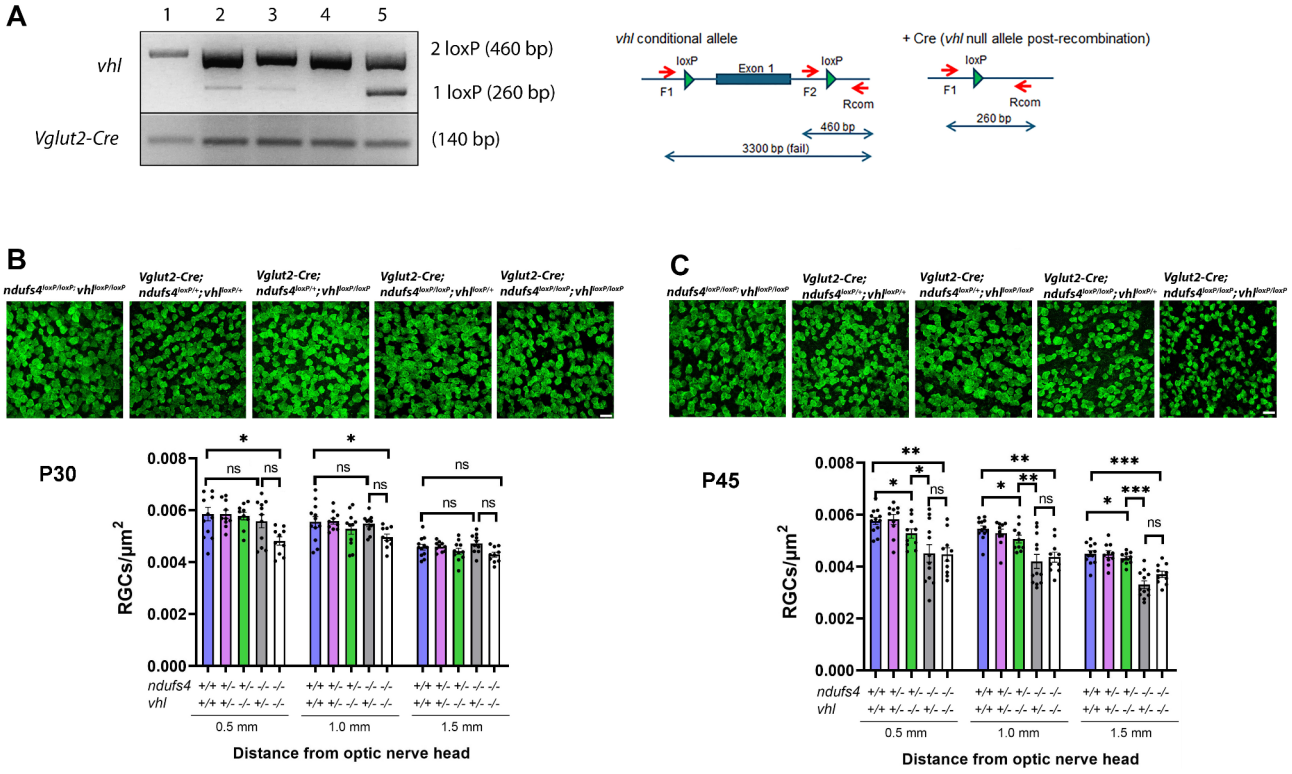

Fig. 3. Neuroprotection of P60 *ndufs4*-deficient retinal ganglion cell somas by hypoxia is not dependent on an intact HIF pathway**.** Representative images of RBPMS1-labeled retinal flat mounts from P60 mice with RGC-specific deletion of both *Hif1α* and *Hif2α*. When the mice are raised under normoxia, the density of RGC somas (immunolabeled for RBPMS1) is reduced in mice that are also homozygous for deletion of *ndufs4* within RGCs (middle panel) compared to those with one intact copy (left panel). With continuous exposure to 11% O_2 beginning at P25, RGCs with homozygous deletion of *ndufs4* (right panel) maintain a normal cell density. Bar, 20 μm. The graph depicts RGC soma density at 0.5, 1.0, and 1.5 mm distances from the optic nerve head, with the RGC *ndufs4* genotype and the ambient O_2 concentration indicated below. Individual data points are overlaid on each bar. Statistical comparisons between groups are indicated above the bars, with the following significance designations: ns, not significant; ***, $p < 0.001$.

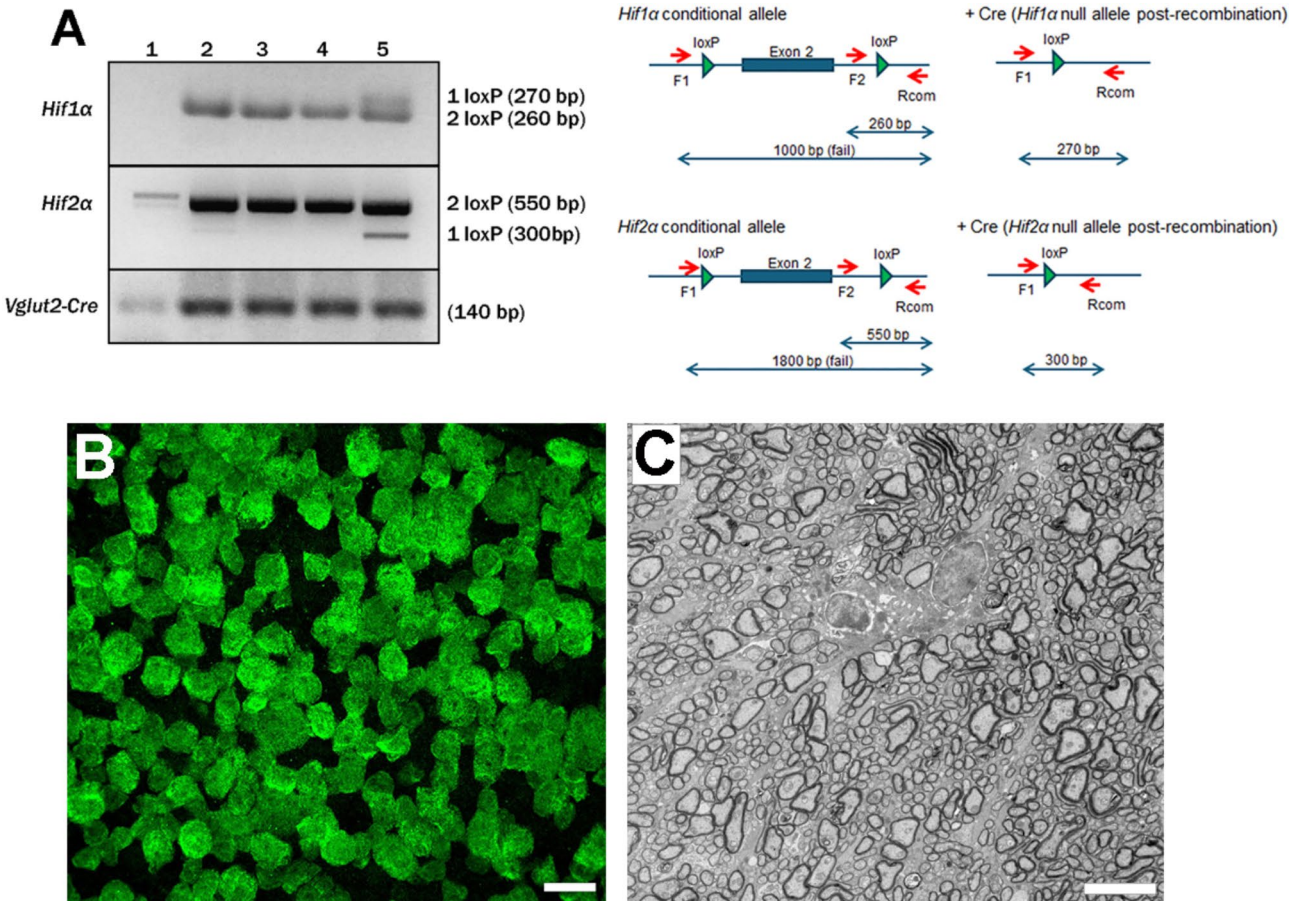

Fig. 4. The partial rescue of *ndufs4*-deficient retinal ganglion cells by hypoxia at P90 is maintained in the absence of an intact HIF pathway**.** (A, B) Representative images of RBPMS1-labeled retinal flat mounts (A) or optic nerve cross sections (B) from P90 mice with RGC-specific homozygous deletion of both *Hif1α* and *Hif2α*. The left panels depict tissue in which there is also heterozygous deletion of *ndufs4* from RGCs, while in the right panels there is homozygous deletion of *ndufs4* from RGCs. From P25 to P90, the mice were raised under 21% O_2 (top panels) or 11% O_2 (bottom panels). Bar, 20 µm. The graphs to the right quantify RGC soma densities at three distances from the optic nerve head (A) and RGC axon densities across entire optic nerve cross sections (B). Individual data points are overlaid on each bar. Statistical comparisons between groups are indicated above the bars, with the following significance designations: ns, not significant; *, $p < 0.05$; **, $p < 0.01$; ***, $p < 0.001$. (C) Electron micrographs of optic nerve cross sections from P90 *Vglut2-Cre; ndufs4*$^{loxP/loxP}$;*Hif1α*$^{loxP/loxP}$;*Hif2α*$^{loxP/loxP}$ mice raised under normoxia (top panels) or hypoxia (bottom panels). Continuous hypoxia reduced RGC axon loss and surrounding fibrosis. The thickening and duplication of myelin sheaths on surviving axons (higher magnification images) were less common in hypoxia-treated mice, but scattered examples were still observed. Black bars, 10 µm. White bars, 0.5 µm.

Discussion

We have demonstrated that the increased survival of complex I-deficient RGCs achieved when mice are raised under continuous hypoxia cannot be recapitulated by genetic ablation of a key negative regulator of the HIF pathway under normoxia and, indeed, appears to be completely independent of the HIF transcription factors. We first found that loss of the HIF negative regulator pVHL within glutamatergic neurons, including RGCs, failed to reduce the degeneration of NDUFS4-deficient RGCs and in fact exacerbated neurological dysfunction in *Vglut2-Cre; ndufs4*$^{loxP/loxP}$ mice, preventing them from surviving to the P60 and P90 time points. This is consistent with the observation by Mootha and colleagues that the lifespan of *ndufs4*$^{-/-}$ mice with global loss of NDUFS4 not only failed to be extended, but in some cases was actually shortened, when combined either with a homozygous *vhl* hypomorphic point mutation or with deletion of any of the three prolyl hydroxylase genes that target HIF proteins for degradation under normoxia[30]. This raises the question of whether the salutary effects of hypoxia in the context of NDUFS4 deficiency may actually occur in spite of, rather than being mediated by, HIF pathway activation. Interestingly, a maladaptive 'pseudohypoxic' state has been reported to occur with aging, in which reduced cellular pVHL levels leads to increased HIF activity under normoxia and results in decreased synthesis of mtDNA-encoded oxidative phosphorylation proteins[37]. A consequent deficiency of additional electron transport chain subunits could easily explain why systemic phenotypes observed with the loss of the nuclear-encoded complex I subunit NDUFS4 are exacerbated by loss of pVHL. However, it should also be noted

that the prolyl hydroxylase enzymes and pVHL also promote the degradation of non-HIF substrates[38,39], so the detrimental effects of their deletion in *ndufs4* knockout models under normoxic conditions may not necessarily be tied to HIF activation. Accordingly, it remained possible that the protective effects of environmental hypoxia might still be mediated by HIF pathway activation, calling for a direct evaluation of the necessity of the HIF transcription factors for RGC rescue by hypoxia.

Because the global loss of HIF-1α or HIF-2α results in embryonic lethality[31,32], the requirement of HIF pathway activation had not previously been tested in mammalian models of complex I deficiency. We determined that simultaneous deletion of both *Hif1α* and *Hif2α* in RGCs had no gross impact on their development or survival, and thus we could combine their cell-specific deletion with that of *ndufs4* in order to formally evaluate the necessity of the HIF pathway in RGC neuroprotection by hypoxia. Using this strategy, we found that rescue of NDUFS4-deficient RGCs by 11% O_2 remained unaffected by genetic ablation of the HIF regulatory pathway. Similar to our previous work in *Vglut2-Cre; ndufs4*$^{loxP/loxP}$ mice with intact *Hif1α* and *Hif2α*, we observed 100% RGC rescue at P60 and > 50% rescue at P90 in *Vglut2-Cre; ndufs4*$^{loxP/loxP}$;*Hif1α*$^{loxP/loxP}$;*Hif2α*$^{loxP/loxP}$ mice exposed to continuous hypoxia prior to the onset of RGC degeneration. This finding is highly consistent with a recent report by Mootha and colleagues that the therapeutic effect of hypoxia in rescuing larval developmental arrest of *C. elegans* mutants lacking the *ndufs4* homolog *lpd-5* is maintained when the HIF homolog *hif-1* is knocked out[40]. Taken together, it appears that activation of the HIF pathway is entirely dispensable to the rescue of complex I deficiency phenotypes by hypoxia and that broadly stimulating this transcriptional program would not be a beneficial therapeutic strategy.

Our findings thus lead to the question of what is the identity of the HIF-independent mechanism(s) mediating the therapeutic effect of hypoxia on complex I-deficient RGCs. One possibility raised by Mootha and colleagues based on their work with the *ndufs4* knockout mouse is that impaired oxidative metabolism caused by complex I dysfunction leads to unused O_2, creating a relative hyperoxic state at the tissue level, which may then be mitigated by exposure to environmental hypoxia[30]. Indeed, tissue hyperoxia could result in oxidative stress, a popular hypothesis to explain cellular dysfunction and death in mitochondrial disease. However, in the case of *Vglut2-Cre; ndufs4*$^{loxP/loxP}$ mice, fewer than 2% of retinal cells (RGCs and a small fraction of cones and horizontal cells) have complex I impairment;[14] given that the vast majority of retinal cells retain normal oxidative metabolic capacity in our model, the development of significant hyperoxia at the tissue level would seem unlikely. Moreover, the Mootha laboratory's recent work in *C. elegans* suggests that reactive oxygen species formation is not related to the pathobiology of larval growth arrest in the *lpd-5* knockout[40]. Rather, they have observed that loss of function of certain complex I subunits, including *lpd-5*, results in an O_2-sensitive decrease in forward electron transfer activity of complex I that may be ameliorated by hypoxia[40]. While these findings are intriguing, the specific cascade of events that results from the decreased electron transfer from complex I to ubiquinone and leads to cellular pathology remains to be determined.

A possible alternative therapeutic mechanism of hypoxia in our model includes an impact on mitochondrial quality control to increase the relative abundance of healthy to unhealthy mitochondria within RGCs. There have been a number of reports suggesting that hypoxia can influence mitochondrial biogenesis, although the data have been conflicting regarding whether hypoxia stimulates or reduces it—likely dependent on the cell type being studied and the duration of hypoxia[41–46]. The activity of PGC1α, the master regulator of mitochondrial biogenesis, is influenced by a number of upstream signaling proteins, several of which (e.g. adenosine monophosphate kinase and sirtuin-1) may stimulate PGC1α under hypoxia[44,47]. Interestingly, the preponderance of evidence suggests that PGC1α activation is independent of, or even inhibited by, the HIF pathway[48,49]. On the other side of the equation, complex I mutations may result in oxidative damage to mitochondrial lipids, proteins, and DNA to produce progressive mitochondrial dysfunction[50,51]. Elimination of damaged mitochondria occurs via mitophagy, a regulated process in which old or unhealthy mitochondria are specifically engulfed within autophagosomes and delivered to lysosomes for degradation[52]. Hypoxia is known to stimulate mitophagy and has been reported to do so via both the HIF pathway and through HIF-independent mechanisms[53–55]. Indeed, a recent in vivo study reported increased mitophagy activity in RGCs that experienced hypoxia as a consequence of elevated intraocular pressure[56]. As demonstrated by our triple knockout of *ndufs4*, *Hif1α* and *Hif2α* within RGCs, our cell-specific mouse model has an advantage of allowing perturbation of key processes such as mitochondrial biogenesis or mitophagy to be studied within RGCs when their ablation may be lethal at the whole organism level.

A significant limitation of our study is that although we demonstrated the deletion of essential exons of *vhl*, *Hif1α* and *Hif2α* within inner retinal cells, we did not directly demonstrate any impact on HIF protein levels or on the expression of HIF target genes. Our approach reflected the challenge of analyzing changes in protein expression in a cell type that is a minor component of a complex tissue like the retina, and our attempts to characterize changes in pVHL and HIF protein levels specifically in RGCs using histological techniques were not successful (data not shown). This problem could be effectively addressed in future studies by employing single cell transcriptional analysis of dissociated retinal cells, an approach that would be enlightening for several reasons. First, the up-regulation of HIF target genes in RGCs lacking pVHL would confirm that HIF stabilization and activation indeed resulted from Cre-mediated *vhl* deletion. Second, a comparison of the expression profiles of RGCs from hypoxia-treated mice with deleted and intact *Hif1α* and *Hif2α* could identify therapeutically-relevant HIF-independent pathways induced within RGCs by environmental hypoxia.

Finally, single cell analysis could be used to explore the possibility that hypoxia may act therapeutically via indirect actions on cells other than RGCs. Neighboring cells that might be relevant in this context include macroglia (Müller cells and astrocytes), amacrine cells, microglia, and infiltrating macrophages. Notably, the genetic approaches to activate and ablate the HIF pathway used in this study would not have affected these other cell types. While we have previously considered the possibility of hypoxia reducing retinal neuro-inflammation in response to mitochondrial dysfunction in RGCs, our prior work demonstrated minimal effect of hypoxia

on the accumulation of Iba1$^+$ mononuclear phagocytic cells (microglia and/or macrophages) in *Vglut2-Cre; ndufs4$^{loxP/loxP}$* retinas[18]. Nevertheless, it is possible that homeostatic vs. neurodegenerative molecular signatures in the phagocytic cells[57,58] could be altered by hypoxia and influence the survival of RGCs with mitochondrial dysfunction. Profiling the effects of hypoxia on non-RGC cell types in the *ndufs4$^{-/-}$* global knockout mouse would also be of interest, given that in mitochondrial diseases like Leber hereditary optic neuropathy, all cells of the body are subject to some level of mitochondrial dysfunction. As such, conducting studies in the setting of global complex I deficiency may allow the identification of important hypoxia-induced physiological changes in non-RGC cell types that could affect the overall disease state.

Methods

Animals

All animal experiments were conducted under a protocol approved by the Institutional Animal Care and Use Committee of Duke University. All methods were performed in accordance with relevant guidelines from the ARVO Statement for the Use of Animals in Ophthalmic and Vision Research. Euthanasia was achieved via inhalation of isoflurane followed by decapitation. The mouse lines used in the described experiments were derived from strains obtained from Jackson Labs. *Vglut2-Cre; ndufs4$^{loxP/loxP}$* mice and control littermates were generated as previously described[14] and were bred with mouse strains bearing *floxed* alleles of *vhl*[24], *Hif1α*[35], and *Hif2α*[36] obtained from Jackson Labs (strain numbers 012933, 007561, 008407, respectively). All genetically modified strains were maintained on a C57Bl/6J background.

Assessment of Cre-mediated DNA recombination in serial tangential retinal sections

To verify successful RGC-specific Cre-mediated recombination of the *floxed vhl*, *Hif1α*, and *Hif2α* alleles, flat-mounted P30 mouse retinas were serially sectioned as previously described[27]. Briefly, 2-mm punches of isolated retinas were obtained using a surgical trephine, transferred photoreceptor-side up to PVDF membrane, flattened between glass slides separated by 0.5 mm spacers, and frozen on dry ice. The flattened retinal specimens were then serially cut into 40-µm-thick sections on a cryostat (CM3050S; Leica), with each section recovered in a separate Eppendorf tube. Genomic DNA was purified from each section using a DNEasy kit (Qiagen). The presence of non-recombined (i.e. bearing 2 LoxP sites) and recombined (1 LoxP site) *floxed* alleles of *vhl*, *Hif1α*, and *Hif2α* allele was determined by PCR, using appropriate primer combinations as described by Barben et al.[26] The sole modification was to the *vhl* Forward-1 primer: ctgcatgcctggtacccacgaaagtg. To compare the extent of Cre-mediated recombination across the full thickness of the retina, PCR products from each serial section were run on a 2% agarose gel.

Continuous hypoxia

To subject mice to continuous hypoxia, cages were kept within an A-Chamber animal cage enclosure (BioSpherix, Ltd., Parish, NY), and the ambient PO_2 was reduced to 11% by pumping in nitrogen gas to displace the oxygen. In these experiments, all mice were born under normoxia, with selected cohorts transferred to the hypoxia chamber at P25 and maintained there until P60 or P90, under a 12-hour light-dark cycle. Those cages housing control littermates were maintained on their original rack under a normoxic 21% O_2 concentration. At the indicated time points, mice were rapidly euthanized upon removal from the hypoxia chamber, followed by harvesting of ocular tissues for histological analyses.

Histological techniques

Immunohistochemistry experiments were performed as previously described[14,59]. Briefly, eyecups obtained from euthanized mice were fixed for 1 h in 4% paraformaldehyde at room temperature. Retinas were isolated, blocked in 5% goat serum in PBS with 0.3% Triton X-100, incubated with rabbit polyclonal anti-RBPMS1 primary antibody (1:500; Novus, NBP2-20112) in block for 5 days at 4 °C, and then incubated with anti-rabbit Alexa Fluor 488 (1:500; Invitrogen) overnight at 4 °C. The retinas were then washed and flat-mounted on glass slides with the RGC layer facing up, with four radial cuts made from the retinal periphery to the equator, dividing each retina into quadrants to assist with flattening prior to mounting under cover slips with Immu-Mount (Thermo Fisher Scientific).

Images were acquired using a Nikon Eclipse Ti2 inverted confocal microscope, a CFI Plan Fluor 60× (oil) objective, and an A1 confocal scanner controlled by NIS-Elements software (Nikon). To quantify RGC somas, 45,000 µm^2 images were obtained in each quadrant at 0.5, 1.0, and 1.5 mm distances from the optic nerve head. RGC somas were manually counted by a masked observer using the Cell Counter plugin for Fiji[60], and the density of the RGC somas was averaged across the four quadrants at each distance from the optic nerve head.

To quantify RGC axons, optic nerves were harvested from the euthanized mice and fixed for two hours at room temperature in 2% paraformaldehyde and 2% glutaraldehyde in PBS. The samples were embedded in Embed-812 resin mixture and cut on an ultramicrotome (LKB Ultratome V; Leica) using a diamond knife to obtain 0.27-µm-thick cross-sections, which were stained with 1% methylene blue. Axon cross section images were obtained using a Nikon Ti2 Eclipse microscope and NIS-Elements imaging software (Nikon). For each optic nerve cross section, 4 images obtained using a 60x (oil) objective and the 1.5x magnifier were stitched in order to capture the entire nerve. This was performed on three cross sections per optic nerve, to verify consistent quantification within each specimen. Axon counts were performed using the AxoNet plugin for ImageJ[61]. The mean RGC axon density per nerve was calculated by averaging the final axon count over each of the three cross-sections per optic nerve specimen, divided by the total optic nerve cross-sectional area.

To prepare optic nerve specimens for transmission electron microscopy, the same tissue blocks were thinly cut into 60–80 nm sections. The sections were collected on copper grids, counterstained with 1% uranyl acetate

and 3.5% lead citrate, and then examined using an electron microscope (JEM-1400; JEOL) at 60 kV. Images were collected using a charge-coupled device camera (Orius; Gatan).

Experimental design and statistical analysis

In all experiments, age-matched mice of both sexes were represented in each cohort. Sufficient numbers of mice were used such that in all histological analyses of RGC soma and axon survival, 8–14 retinas or optic nerves were analyzed for each mouse genotype and O_2 concentration at each time point. Randomization of mice to each experimental group was driven by Mendelian inheritance; where relevant, the initiation of exposure to hypoxia occurred prior to the development of any overt phenotypes in the mice. Each eye was analyzed for every mouse, with specimens excluded only if a mouse exhibited evidence of ocular trauma or if tissue was damaged during harvesting. Quantitative analysis of RGC survival in histological specimens was performed in a masked manner. Statistical comparisons between groups were made with the Wilcoxon rank sum test to account for non-parametric data. All data analysis for this study was generated using SAS/STAT software, Version 9.4 of the SAS System for Windows (SAS Institute, Inc.). Data are presented graphically as mean ± SEM. The study is reported in accordance with ARRIVE guidelines.

Data availability

The datasets generated during and/or analyzed during the current study are available from the corresponding author on reasonable request.

Received: 7 April 2024; Accepted: 9 October 2024
Published online: 15 October 2024

References

1. Finsterer, J., Mancuso, M., Pareyson, D., Burgunder, J. M. & Klopstock, T. Mitochondrial disorders of the retinal ganglion cells and the optic nerve. *Mitochondrion*. **42**, 1–10 (2018).
2. Wang, M. Y. & Sadun, A. A. Drug-related mitochondrial optic neuropathies. *J. Neuroophthalmol.* **33**, 172–178 (2013).
3. Sadun, A. A. Metabolic optic neuropathies. *Semin Ophthalmol.* **17**, 29–32 (2002).
4. Barot, M., Gokulgandhi, M. R. & Mitra, A. K. Mitochondrial dysfunction in retinal diseases. *Curr. Eye Res.* **36**, 1069–1077 (2011).
5. Sundaramurthy, S. et al. Leber hereditary optic neuropathy-new insights and old challenges. *Graefes Arch. Clin. Exp. Ophthalmol.* **259**, 2461–2472 (2021).
6. Yu-Wai-Man, P. et al. The epidemiology of leber hereditary optic neuropathy in the north east of England. *Am. J. Hum. Genet.* **72**, 333–339 (2003).
7. Fraser, J. A., Biousse, V. & Newman, N. J. The neuro-ophthalmology of mitochondrial disease. *Surv. Ophthalmol.* **55**, 299–334 (2010).
8. Wong, A. et al. Differentiation-specific effects of lhon mutations introduced into neuronal nt2 cells. *Hum. Mol. Genet.* **11**, 431–438 (2002).
9. Baracca, A. et al. Severe impairment of complex i-driven adenosine triphosphate synthesis in leber hereditary optic neuropathy cybrids. *Arch. Neurol.* **62**, 730–736 (2005).
10. Tonska, K., Kodron, A. & Bartnik, E. Genotype-phenotype correlations in leber hereditary optic neuropathy. *Biochim. Biophys. Acta*. **1797**, 1119–1123 (2010).
11. Lin, C. S. et al. Mouse mtdna mutant model of leber hereditary optic neuropathy. *Proc. Natl. Acad. Sci. U S A*. **109**, 20065–20070 (2012).
12. Yu, H. et al. Consequences of zygote injection and germline transfer of mutant human mitochondrial DNA in mice. *Proc. Natl. Acad. Sci. U S A*. **112**, E5689–5698 (2015).
13. Yu, H., Sant, D. W., Wang, G. & Guy, J. Mitochondrial transfer of the mutant human nd6t14484c gene causes visual loss and optic neuropathy. *Transl Vis. Sci. Technol.* **9**, 1 (2020).
14. Wang, L. et al. Progressive optic atrophy in a retinal ganglion cell-specific mouse model of complex i deficiency. *Sci. Rep.* **10**, 16326 (2020).
15. Ferrari, M. et al. Hypoxia treatment reverses neurodegenerative disease in a mouse model of leigh syndrome. *Proc. Natl. Acad. Sci. U S A*. **114**, E4241–E4250 (2017).
16. Grange, R. M. H. et al. Hypoxia ameliorates brain hyperoxia and nad(+) deficiency in a murine model of leigh syndrome. *Mol. Genet. Metab.* **133**, 83–93 (2021).
17. Jain, I. H. et al. Hypoxia as a therapy for mitochondrial disease. *Science*. **352**, 54–61 (2016).
18. Warwick, A. M. et al. Continuous hypoxia reduces retinal ganglion cell degeneration in a mouse model of mitochondrial optic neuropathy. *Invest. Ophthalmol. Vis. Sci.* **63**, 21 (2022).
19. Wenger, R. H. Cellular adaptation to hypoxia: O2-sensing protein hydroxylases, hypoxia-inducible transcription factors, and o2-regulated gene expression. *FASEB J.* **16**, 1151–1162 (2002).
20. Albadari, N., Deng, S. & Li, W. The transcriptional factors hif-1 and hif-2 and their novel inhibitors in cancer therapy. *Expert Opin. Drug Discov.* **14**, 667–682 (2019).
21. Hu, C. J., Wang, L. Y., Chodosh, L. A., Keith, B. & Simon, M. C. Differential roles of hypoxia-inducible factor 1alpha (hif-1alpha) and hif-2alpha in hypoxic gene regulation. *Mol. Cell. Biol.* **23**, 9361–9374 (2003).
22. Jaakkola, P. et al. Targeting of hif-alpha to the Von hippel-lindau ubiquitylation complex by o2-regulated prolyl hydroxylation. *Science*. **292**, 468–472 (2001).
23. Gnarra, J. R. et al. Defective placental vasculogenesis causes embryonic lethality in vhl-deficient mice. *Proc. Natl. Acad. Sci. U S A*. **94**, 9102–9107 (1997).
24. Haase, V. H., Glickman, J. N., Socolovsky, M. & Jaenisch, R. Vascular tumors in livers with targeted inactivation of the Von hippel-lindau tumor suppressor. *Proc. Natl. Acad. Sci. U S A*. **98**, 1583–1588 (2001).
25. Jeon, C. J., Strettoi, E. & Masland, R. H. The major cell populations of the mouse retina. *J. Neurosci.* **18**, 8936–8946 (1998).
26. Barben, M. et al. Hif1a inactivation rescues photoreceptor degeneration induced by a chronic hypoxia-like stress. *Cell. Death Differ.* **25**, 2071–2085 (2018).
27. Sokolov, M. et al. Massive light-driven translocation of transducin between the two major compartments of rod cells: a novel mechanism of light adaptation. *Neuron*. **34**, 95–106 (2002).
28. Schlamp, C. L. et al. Evaluation of the percentage of ganglion cells in the ganglion cell layer of the rodent retina. *Mol. Vis.* **19**, 1387–1396 (2013).
29. Bolea, I. et al. Defined neuronal populations drive fatal phenotype in a mouse model of leigh syndrome. *Elife.* **8**, e47163 (2019).

30. Jain, I. H. et al. Leigh syndrome mouse model can be rescued by interventions that normalize brain hyperoxia, but not hif activation. *Cell. Metab.* **30**, 824–832e823 (2019).
31. Iyer, N. V. et al. Cellular and developmental control of o2 homeostasis by hypoxia-inducible factor 1 alpha. *Genes Dev.* **12**, 149–162 (1998).
32. Tian, H., Hammer, R. E., Matsumoto, A. M., Russell, D. W. & McKnight, S. L. The hypoxia-responsive transcription factor epas1 is essential for catecholamine homeostasis and protection against heart failure during embryonic development. *Genes Dev.* **12**, 3320–3324 (1998).
33. Duan, C. Hypoxia-inducible factor 3 biology: complexities and emerging themes. *Am. J. Physiol. Cell. Physiol.* **310**, C260–269 (2016).
34. Barteczek, P. et al. Neuronal hif-1alpha and hif-2alpha deficiency improves neuronal survival and sensorimotor function in the early acute phase after ischemic stroke. *J. Cereb. Blood Flow. Metab.* **37**, 291–306 (2017).
35. Ryan, H. E. et al. Hypoxia-inducible factor-1alpha is a positive factor in solid tumor growth. *Cancer Res.* **60**, 4010–4015 (2000).
36. Gruber, M. et al. Acute postnatal ablation of hif-2alpha results in anemia. *Proc. Natl. Acad. Sci. U S A.* **104**, 2301–2306 (2007).
37. Gomes, A. P. et al. Declining nad(+) induces a pseudohypoxic state disrupting nuclear-mitochondrial communication during aging. *Cell.* **155**, 1624–1638 (2013).
38. Zhang, J. & Zhang, Q. Vhl and hypoxia signaling: beyond hif in cancer. *Biomedicines.* **6**, 35 (2018).
39. Strowitzki, M. J., Cummins, E. P. & Taylor, C. T. Protein hydroxylation by hypoxia-inducible factor (hif) hydroxylases: Unique or ubiquitous? *Cells* 8 (2019).
40. Meisel, J. D. et al. Hypoxia and intra-complex genetic suppressors rescue complex i mutants by a shared mechanism. *Cell.* **187**, 659–675 (2024).
41. Qian, X. et al. Kdm3a senses oxygen availability to regulate pgc-1alpha-mediated mitochondrial biogenesis. *Mol. Cell.* **76**, 885–895e887 (2019).
42. Zhu, L. et al. Hypoxia induces pgc-1alpha expression and mitochondrial biogenesis in the myocardium of tof patients. *Cell. Res.* **20**, 676–687 (2010).
43. Gutsaeva, D. R. et al. Transient hypoxia stimulates mitochondrial biogenesis in brain subcortex by a neuronal nitric oxide synthase-dependent mechanism. *J. Neurosci.* **28**, 2015–2024 (2008).
44. Shoag, J. & Arany, Z. Regulation of hypoxia-inducible genes by pgc-1 alpha. *Arterioscler. Thromb. Vasc Biol.* **30**, 662–666 (2010).
45. Tohme, S. et al. Hypoxia mediates mitochondrial biogenesis in hepatocellular carcinoma to promote tumor growth through hmgb1 and tlr9 interaction. *Hepatology*. **66**, 182–197 (2017).
46. Yun, C. W., Lee, J. H. & Lee, S. H. Hypoxia-induced pgc-1alpha regulates mitochondrial function and tumorigenesis of colorectal cancer cells. *Anticancer Res.* **39**, 4865–4876 (2019).
47. Gao, J., Qian, T. & Wang, W. Ctrp3 activates the ampk/sirt1-pgc-1alpha pathway to protect mitochondrial biogenesis and functions in cerebral ischemic stroke. *Neurochem Res.* **45**, 3045–3058 (2020).
48. Arany, Z. et al. Hif-independent regulation of vegf and angiogenesis by the transcriptional coactivator pgc-1alpha. *Nature*. **451**, 1008–1012 (2008).
49. LaGory, E. L. et al. Suppression of pgc-1alpha is critical for reprogramming oxidative metabolism in renal cell carcinoma. *Cell. Rep.* **12**, 116–127 (2015).
50. Wallace, D. C. & Fan, W. The pathophysiology of mitochondrial disease as modeled in the mouse. *Genes Dev.* **23**, 1714–1736 (2009).
51. Guo, C., Sun, L., Chen, X. & Zhang, D. Oxidative stress, mitochondrial damage and neurodegenerative diseases. *Neural Regen Res.* **8**, 2003–2014 (2013).
52. Okamoto, K. & Organellophagy Eliminating cellular building blocks via selective autophagy. *J. Cell. Biol.* **205**, 435–445 (2014).
53. Wu, H. & Chen, Q. Hypoxia activation of mitophagy and its role in disease pathogenesis. *Antioxid. Redox Signal.* **22**, 1032–1046 (2015).
54. Daskalaki, I., Gkikas, I. & Tavernarakis, N. Hypoxia and selective autophagy in cancer development and therapy. *Front. Cell. Dev. Biol.* **6**, 104 (2018).
55. Papandreou, I., Lim, A. L., Laderoute, K. & Denko, N. C. Hypoxia signals autophagy in tumor cells via ampk activity, independent of hif-1, bnip3, and bnip3l. *Cell. Death Differ.* **15**, 1572–1581 (2008).
56. Morgan, A. B., Fan, Y. & Inman, D. M. The ketogenic diet and hypoxia promote mitophagy in the context of glaucoma. *Front. Cell. Neurosci.* **18**, 1409717 (2024).
57. Butovsky, O. et al. Identification of a unique tgf-beta-dependent molecular and functional signature in microglia. *Nat. Neurosci.* **17**, 131–143 (2014).
58. Krasemann, S. et al. The trem2-apoe pathway drives the transcriptional phenotype of dysfunctional microglia in neurodegenerative diseases. *Immunity*. **47**, 566–581e569 (2017).
59. Gospe, S. M. et al. 3rd Photoreceptors in a mouse model of leigh syndrome are capable of normal light-evoked signaling. *J Biol Chem* 294, 12432–12443 (2019).
60. Schindelin, J. et al. Fiji: an open-source platform for biological-image analysis. *Nat. Methods*. **9**, 676–682 (2012).
61. Ritch, M. D. et al. Axonet: a deep learning-based tool to count retinal ganglion cell axons. *Sci. Rep.* **10**, 8034 (2020).

Acknowledgements

This work was funded by the National Eye Institute via grants EY028610 (S.M.G.) and Core Grant EY005722 (Duke University), a Duke University School of Medicine Strong Start Award (S.M.G.), and an Unrestricted Research to Prevent Blindness Grant (Duke Eye Center).

Author contributions

SMG designed the research; AMW, HMB, LW, and YH performed the research; AMW, HMB, LW, SSS, and SMG analyzed the data; SMG wrote the main manuscript text; and all authors reviewed and approved the manuscript.

Declarations

Competing interests

The authors declare no competing interests.

Additional information

Supplementary Information The online version contains supplementary material available at https://doi.org/10.1038/s41598-024-75916-x.

Correspondence and requests for materials should be addressed to S.M.G.